

Wafer-scale Heterogeneous Integration of Monocrystalline β -Ga₂O₃ Thin Films on SiC for Thermal Management by Ion-Cutting Technique

Zhe Cheng^{1,a)}, Fengwen Mu^{2,4,a),*}, Tianguai You^{3,a)}, Wenhui Xu³, Jingjing Shi¹, Michael E. Liao⁵, Yekan Wang⁵, Kenny Huynh⁵, Tadatomo Suga⁴, Mark S. Goorsky⁵, Xin Ou^{3,*}, Samuel Graham^{1,6,*}

¹ George W. Woodruff School of Mechanical Engineering, Georgia Institute of Technology, Atlanta, Georgia 30332, USA

² Kagami Memorial Research Institute for Materials Science and Technology, Waseda University, Shinjuku, Tokyo 169-0051, Japan

³ State Key Laboratory of Functional Materials for Informatics, Shanghai Institute of Microsystem and Information Technology, Chinese Academy of Sciences, 200050, China

⁴ Collaborative Research Center, Meisei University, Hino-shi, Tokyo 191-8506, Japan

⁵ Materials Science and Engineering, University of California, Los Angeles, Los Angeles, CA, 90095, United States

⁶ School of Materials Science and Engineering, Georgia Institute of Technology, Atlanta, Georgia 30332, USA

^{a)} These authors contributed equally

* Corresponding authors: mufengwen123@gmail.com; ouxin@mail.sim.ac.cn;

sgraham@gatech.edu

Abstract

The ultra-wide bandgap, high breakdown electric field, and large-area affordable substrates make β -Ga₂O₃ promising for applications of next-generation power electronics while its thermal conductivity is at least one order of magnitude lower than other wide/ultrawide bandgap semiconductors. To avoid the degradation of device performance and reliability induced by the localized Joule-heating, aggressive thermal management strategies are essential, especially for high-power high-frequency applications. This work reports a scalable thermal management strategy to heterogeneously integrate wafer-scale monocrystalline β -Ga₂O₃ thin films on high thermal conductivity SiC substrates by ion-cutting technique. The thermal boundary conductance (TBC) of the β -Ga₂O₃-SiC interfaces and thermal conductivity of the β -Ga₂O₃ thin films were measured by Time-domain Thermoreflectance (TDTR) to evaluate the effects of interlayer thickness and thermal annealing. Materials characterizations were performed to understand the mechanisms of thermal transport in these structures. The results show that the β -Ga₂O₃-SiC TBC values increase with decreasing interlayer thickness and the β -Ga₂O₃ thermal conductivity increases more than twice after annealing at 800 °C due to the removal of implantation-induced strain in the films. A Callaway model is built to understand the measured thermal conductivity. Small spot-to-spot variations of both TBC and Ga₂O₃ thermal conductivity confirm the uniformity and high-quality of the bonding and exfoliation. Our work paves the way for thermal management of power electronics and β -Ga₂O₃ related semiconductor devices.

Due to the ultra-wide bandgap (4.8 eV), high breakdown electric field (8 MV/cm), and large-area affordable substrates grown from melt, β -Ga₂O₃ has attracted great attention for potential applications of next-generation power electronics recently.¹⁻⁴ The Baliga figure of merit of β -Ga₂O₃ is several orders of magnitude higher than that of Si.^{3,5,6} However, the thermal conductivity of bulk β -Ga₂O₃ is at least one order of magnitude lower than those of other wide bandgap semiconductors and is highly anisotropic due to the low (monoclinic) crystal structure.⁷⁻¹⁰ Moreover, the thermal conductivity of β -Ga₂O₃ nanostructures, such as thin films, superlattice, and nanocrystalline films, is further significantly reduced compared with that of the bulk β -Ga₂O₃.^{7,11,12} For high-frequency and high-power applications, the device performance and reliability are limited by the high channel temperature induced by the localized Joule-heating near the gate. Therefore, proper, even aggressive, thermal management is of great importance to avoid device degradation.⁴ However, compared with current demonstrations of β -Ga₂O₃ devices, a disproportionately small amount of work is addressing this sensitive issue.⁴

To extract the heat out of power electronic devices, high thermal conductivity substrates or top metal contacts with high thermal boundary conductance (TBC) near the gate are favorable.^{10,13,14} However, direct growth of high-quality β -Ga₂O₃ on high thermal conductivity substrates such as diamond and SiC is difficult due to the differences in crystal symmetry between β -Ga₂O₃ and substrates.¹² Recently, devices based on mechanically exfoliated monocrystalline β -Ga₂O₃ nano-membranes have been fabricated and a record high drain current has been achieved via van der Waals bonding with single crystalline diamond.¹⁵⁻¹⁹ These works demonstrated the great potential of β -Ga₂O₃ devices. However, these devices have limited capability to scale up to wafer-scale

fabrications. Moreover, the van der Waals bonding leads to a low TBC between β -Ga₂O₃ and the substrates, which hinders the cooling effect of the high thermal conductivity substrates.¹¹

In this work, we report a scalable wafer-scale strategy to heterogeneously integrate nanoscale monocrystalline β -Ga₂O₃ thin films on high thermal conductivity SiC substrates via ion-cutting and surface-activated bonding techniques. Time-domain thermoreflectance (TDTR) is used to measure the thermal conductivity of the β -Ga₂O₃ thin films and the TBC of the β -Ga₂O₃-SiC interfaces. Detailed materials characterizations such as a transmission electron microscopy (TEM), High resolution X-ray diffraction (HRXRD), and electron energy loss spectroscopy (EELS) are performed to study the structure-property relation of the β -Ga₂O₃ thin films and the interfaces. Additionally, we build some thermal models to understand the measured thermal conductivity and TBC.

Results

Four samples (10 mm x 8 mm) were prepared in this work, as shown in the schematic diagram of Figure 1. 2-inch bulk (201) β -Ga₂O₃ wafers were implanted with hydrogen ions. A layer of Al₂O₃ is deposited on the β -Ga₂O₃ wafers by atomic layer deposition (ALD) before bonding to a 4-inch 4H-SiC wafer at room temperature via the surface activated bonding technique. The Al₂O₃ layers are used to block the electrical breakdown due to the interface defects in devices while they induce additional thermal resistance. After that, a thin layer of monocrystalline β -Ga₂O₃ was exfoliated from the bulk β -Ga₂O₃ wafer by annealing. The β -Ga₂O₃ wafers can be used for multiple exfoliations, which save materials and lower the fabrication cost. More details about the sample preparation can be found in the Methods section. We name the four samples as Samp1, Samp2,

Samp3, and Samp4. Samp1 and Samp2 have 30-nm- Al_2O_3 interlayers while Samp3 and Samp4 have 10-nm- Al_2O_3 interlayers. Samp1 and Samp3 are as-bonded while Samp2 and Samp4 were annealed at 800 °C in N_2 .

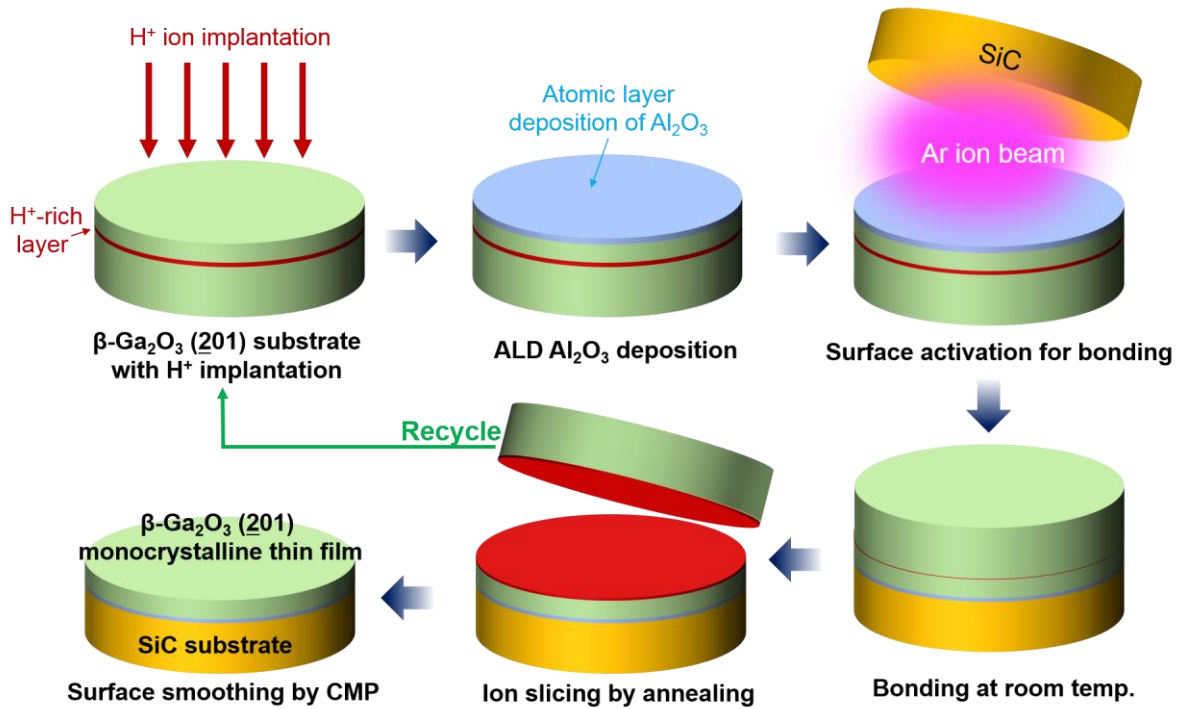


Figure 1. Schematic diagram of sample preparation. A layer of Al_2O_3 is deposit on the $\beta\text{-Ga}_2\text{O}_3$ wafer which is implanted by H ions. After that, surface activated bonding is used to bond the Al_2O_3 coated $\beta\text{-Ga}_2\text{O}_3$ wafer with a 4H-SiC wafer at room temperature. A thin layer of monocrystalline $\beta\text{-Ga}_2\text{O}_3$ is transferred on the SiC wafer after heating up to 450 °C. The surface can be smoothed by chemical mechanical polishing (CMP) and the rest of the $\beta\text{-Ga}_2\text{O}_3$ wafer can be repeatedly used.

Figure 2 (a) shows a 2-inch (201) $\beta\text{-Ga}_2\text{O}_3$ wafer bonded with a 4-inch 4H-SiC wafer. We can see the excellent quality of the wafer bonding. No voids are observed in the bonded area. Our work brings the bulk-quality monocrystalline (201) $\beta\text{-Ga}_2\text{O}_3$ directly bonded to high thermal

conductivity SiC. Figure 2(b) shows the image of the monocrystalline (201) β -Ga₂O₃ transferred onto the 4H-SiC substrate. Only a monocrystalline nanoscale thin film (~140 nm thick) remains on the SiC wafer, which allows for later device fabrication or homo-epitaxial growth of β -Ga₂O₃ structures on these β -Ga₂O₃-on-SiC wafers. We did not see any voids on these exfoliated β -Ga₂O₃ thin films, which confirms the high-quality bonding and exfoliation. Furthermore, the bulk (201) β -Ga₂O₃ wafer can be repeatedly used for multiple exfoliations.

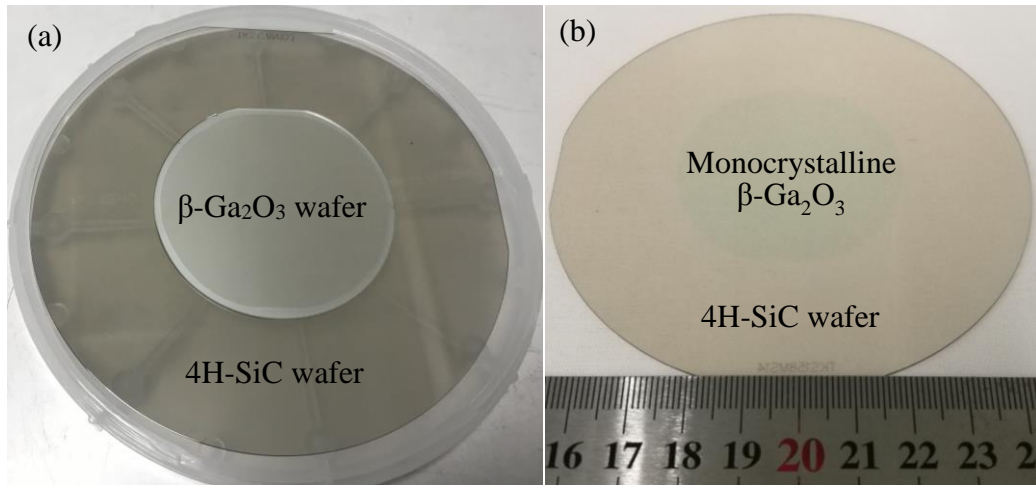


Figure 2. (a) A 2-inch β -Ga₂O₃ wafer is bonded on a 4-inch 4H-SiC wafer. (b) The monocrystalline β -Ga₂O₃ thin film is transferred onto the 4H-SiC wafer.

To evaluate the heat dissipation capability of these β -Ga₂O₃-on-SiC wafers, we measured the thermal boundary conductance (TBC) of the β -Ga₂O₃-SiC interfaces and the thermal conductivity of the β -Ga₂O₃ thin films by TDTR. TDTR is an optical pump-probe technique for thermal characterization of both bulk and nanostructured materials.^{9,20-22} More details about the TDTR measurements can be found in the Methods section. Here, we will discuss the β -Ga₂O₃-SiC TBC first. As shown in Figure 3(a), the samples have three layers: Al transducer, β -Ga₂O₃ layer and SiC substrate. Here, the measured TBC is an effective TBC which includes the thermal resistance of

the β -Ga₂O₃-Al₂O₃ interface, the Al₂O₃-interlayer, and the Al₂O₃-SiC interface. The TBC of the four samples were measured to evaluate the effects of Al₂O₃ thickness and annealing. Figure 3(b) shows the β -Ga₂O₃-SiC TBC of Samp1 (30 nm Al₂O₃ interlayer, as-bonded) and Samp2 (30 nm Al₂O₃ interlayer, annealed at 800 °C in N₂). 14 arbitrarily selected spots were measured on each sample to check the uniformity of the bonding. The TBC variations are less than 6%, which confirms the uniformity of the bonded interfaces. Figure 3(c) shows the measured β -Ga₂O₃-SiC TBC of Samp3 (10 nm Al₂O₃ interlayer, as-bonded) and Samp4 (10 nm Al₂O₃ interlayer, annealed at 800 °C in N₂). Uniform TBC is also observed for four different randomly selected spots on the samples. The β -Ga₂O₃-SiC TBC of Samp3 and Samp4 are larger than those of Samp1 and Samp2 with thicker Al₂O₃ interlayers. Al₂O₃ interlayers induce additional thermal resistances at the β -Ga₂O₃-SiC interfaces so thinner interlayers lead to smaller thermal resistances and larger effective TBC. The TBC of the as-bonded, unannealed samples are slightly larger than those of the annealed interfaces.

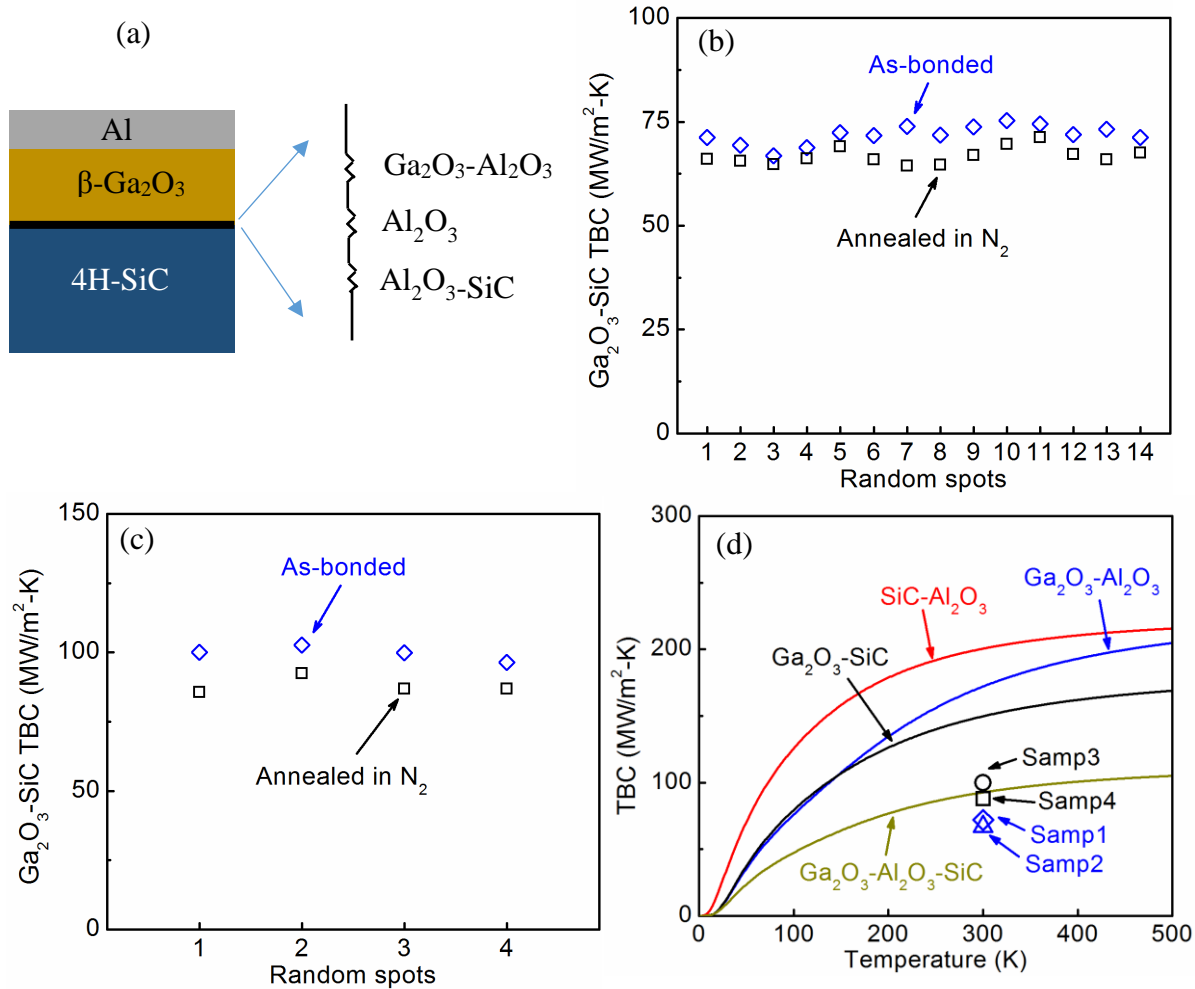


Figure 3. (a) The schematic diagram of the sample structure and thermal resistance. (b) The measured β -Ga₂O₃-SiC TBC of Samp1 and Samp2 which have 30 nm Al₂O₃ interlayers. 14 different spots were measured to show the uniformity of the samples. (c) The measured β -Ga₂O₃-SiC TBC of Samp3 and Samp4 which have 10 nm Al₂O₃ interlayers. (d) Comparison of measured TBC and calculated TBC.

Figure 3(d) shows the comparison of the measured TBC of the four samples and calculated temperature dependent TBC of β -Ga₂O₃-SiC interfaces, β -Ga₂O₃-Al₂O₃ interfaces, and Al₂O₃-SiC interfaces. Density-functional-theory is used to calculate the phonon dispersion relation of the β -

Ga₂O₃, Al₂O₃, and 4H-SiC. Diffuse mismatch model (DMM) is used to calculate the phonon transmission and the TBC can be evaluated by the Landauer Formula.^{11,23} The detailed derivation and formula used to do this calculation can be found in the Methods section. The β -Ga₂O₃-SiC and Ga₂O₃-Al₂O₃ TBC are not very large due to the small phonon group velocity (6620 m/s) of β -Ga₂O₃ in the direction perpendicular to (201) plane.^{11,24} The β -Ga₂O₃-Al₂O₃-SiC TBC is an effective TBC which considers the thermal resistance of both the β -Ga₂O₃-Al₂O₃ interface and the Al₂O₃-SiC interface: $1/\text{TBC}(\beta\text{-Ga}_2\text{O}_3\text{-Al}_2\text{O}_3\text{-SiC})=1/\text{TBC}(\beta\text{-Ga}_2\text{O}_3\text{-Al}_2\text{O}_3)+1/\text{TBC}(\text{Al}_2\text{O}_3\text{-SiC})$. We see good agreement between of the measured TBC and calculated TBC at room temperature. Please note that the DMM-based Landauer formula is only an estimate of the TBC and does not capture exact physics near the interface.

To understand the measured TBC, TEM is used to characterize the interfacial structure. Figure 4(a-b) shows the interfacial structures of Samp1 and Samp2. The β -Ga₂O₃ is very well-bonded with the SiC wafer without any voids. The β -Ga₂O₃-Al₂O₃ interfaces are very smooth and both sides of these interfaces are crystalline materials, while there are amorphous layers at the Al₂O₃-SiC interfaces. These amorphous layers result from the surface activation by Ar ions during the surface activated bonding process. By comparing Samp1 and Samp2, the annealing process makes the amorphous layers slightly thinner (from ~3.5 nm to ~2 nm), which facilitates thermal transport across interfaces. Also, annealing can possibly improve the crystalline quality of the Al₂O₃ interlayers, which facilitates thermal transport as well. However, we observed a slightly reduced TBC, especially for Samp3 and Samp4.

To figure out the potential mechanisms of the reduced TBC after annealing (comparison of Samp3 and Samp4), STEM and EELS were performed to study the interfacial structures of Samp3 and Samp4, as shown in Figure 4(c-f). Figure 4 (c-d) show the STEM bright-field (BF) images of the β -Ga₂O₃-SiC interfaces of Samp3 and Samp4, respectively. The interfaces consist of ~9-nm-thick ALD-Al₂O₃ layers and ~2-nm amorphous SiC layers. Similar to the amorphous layers in Samp1 and Samp2, these amorphous layers result from the surface activation by the Ar ion beams. The ions impact the SiC surface and break the bonds near the surface, which turns the crystalline SiC into amorphous SiC. Figure 4 (e-f) show the EELS mapping of Ga element distributions of the interface of Samp3 and Samp4. Ga element or GaO_x diffusion into the Al₂O₃ interlayers to form AlGaO alloys is observed after annealing in N₂ gas at 800 °C. Alloy structure scatters phonons extensively and reduce thermal conductivity. We attribute this alloy effect as the possible reason for the slightly reduced TBC measured by TDTR.

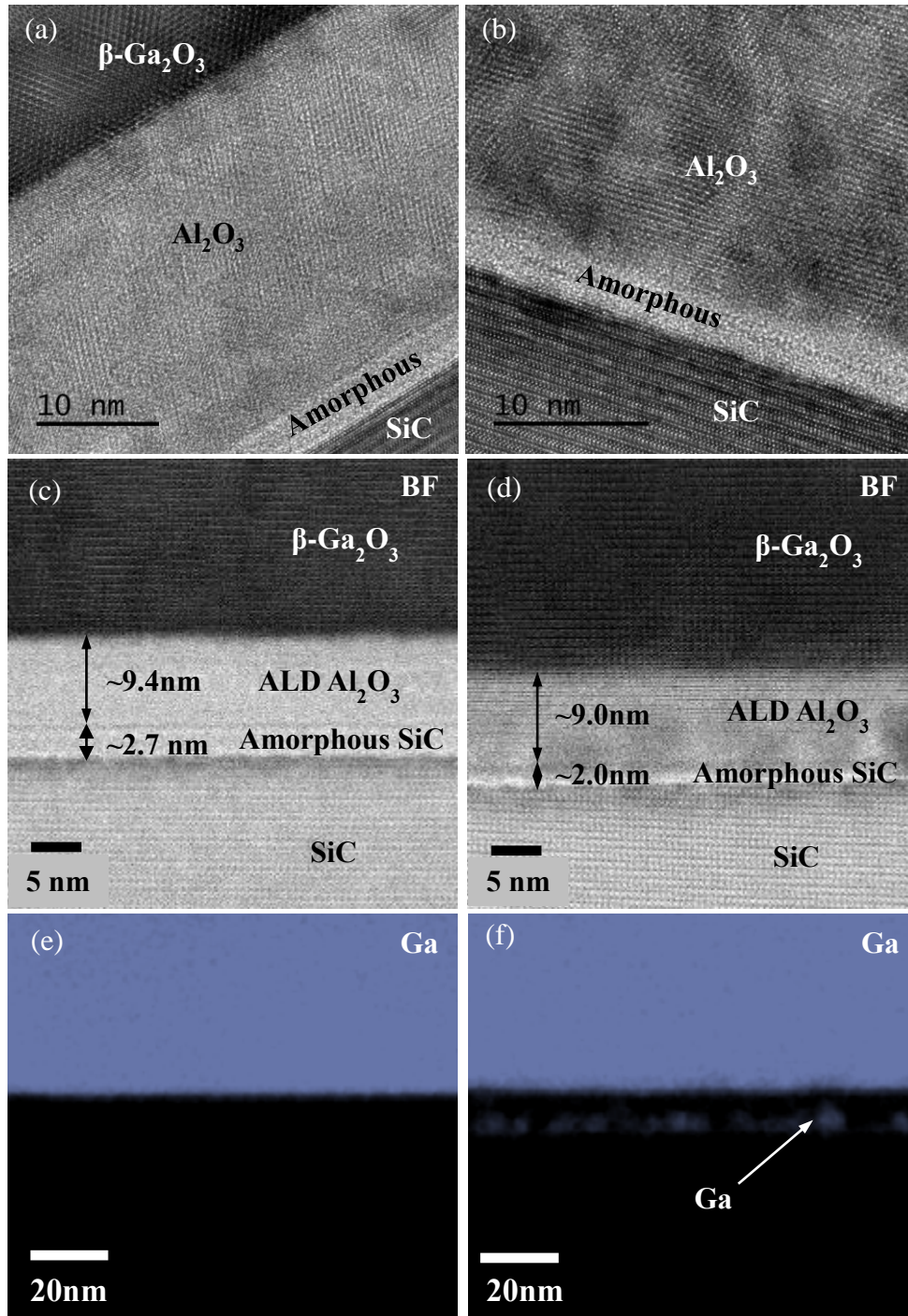


Figure 4. (a) HRTEM images of Samp1 with a 30 nm Al_2O_3 interlayer (as-bonded). (b) HRTEM images of Samp2 with a 30 nm Al_2O_3 interlayer (annealed). (c) STEM images of the interface of Samp3 with a 10 nm Al_2O_3 interlayer (as-bonded). (d) STEM images of the interface of Samp4 with a 10-nm Al_2O_3 interlayer (annealed). (e) Ga element EELS map of the interface of Samp3.

(f) Ga EELS map of the interface of Samp4. Ga diffusion is observed after annealing in N₂ gas at 800 °C.

The thermal conductivity of the monocrystalline nanoscale β -Ga₂O₃ thin films were also measured by TDTR, as shown in Figure 5. Figure 5(a) shows the measured thermal conductivity of β -Ga₂O₃ thin films of Samp1 and Samp2 while Figure 5(b) shows those of Samp3 and Samp4. 14 random spots were measured to check the uniformity of the β -Ga₂O₃ thin films. The small variation of the measured thermal conductivity confirms the uniformity of these thin films. The measured thermal conductivity of the monocrystalline (201) β -Ga₂O₃ thin films (2.9 W/m-K) is more than four times lower than the bulk counterpart (13.3 W/m-K).²⁴ The significant reduction in thermal conductivity is due to the film boundary scattering and the implantation-induced strain in the thin films, which will be discussed in detail later.²⁵ The thermal conductivity of the β -Ga₂O₃ thin films increases more than twice after annealing in N₂. Annealing reduces the implant-induced strain in the thin films. As shown in Figure 5(b), a similar increase in the thermal conductivity of the β -Ga₂O₃ thin films was observed in Samp3 and Samp4.

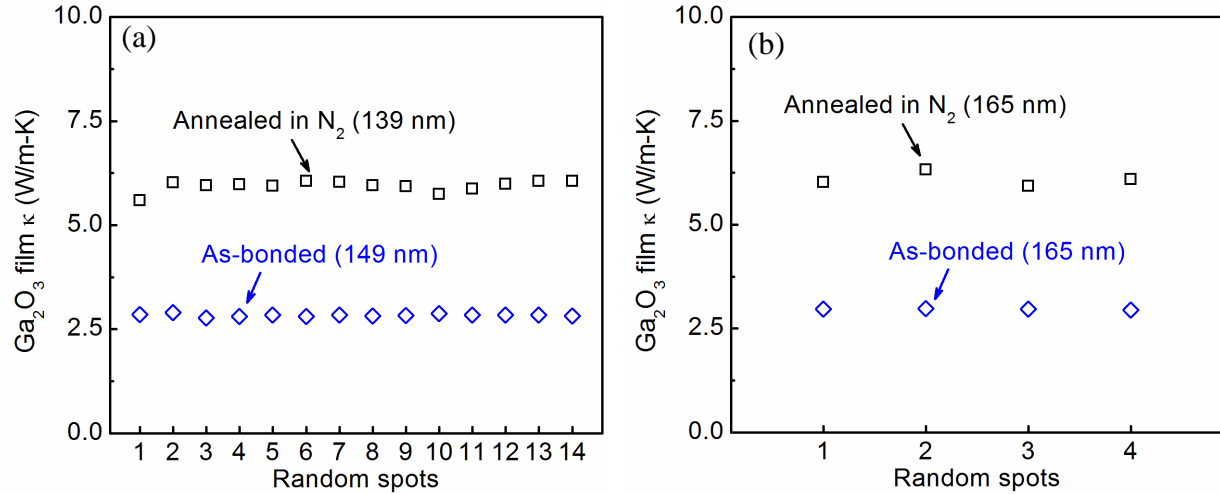


Figure 5. (a) The measured thermal conductivity of β -Ga₂O₃ thin films of Samp1 and Samp2. (b) The measured thermal conductivity of β -Ga₂O₃ thin films of Samp3 and Samp4.

To evaluate the strain variation before and after annealing in N₂, we performed triple-axis XRD measurements on Samp1 and Samp2, as shown in Figure 6(a-b). For the as-bonded sample, the strain from implantation is not completely removed while all strain is removed for the annealed samples. This is similar to other implanted materials.^{25,26} Figure 6(a) is the triple-axis diffraction and the peaks are relative to the (0004) 4H-SiC. The peaks near $\sim -30,000$ arcsec are from the β -Ga₂O₃ layers; this large offset shows the angular difference between the (201) β -Ga₂O₃ peak and the (0004) 4H-SiC peak. Samp1 shows an asymmetric peak and is shifted to a lower angle (larger out-of-plane lattice parameter as expected for implanted material) from the expected lattice parameter of β -Ga₂O₃. The fringe period corresponds to a thickness of ~ 140 nm, which agrees with the thicknesses measured by TEM. Samp2 shifts to the smaller angle expected for (201) β -Ga₂O₃ and shows a symmetric peak with a fringe period that also corresponds to ~ 140 nm.

Figure 6(b) shows the rocking curves of Samp1 (as-bonded) and Samp2 (annealed at 800 °C in N₂). The FWHM of Samp1 is 170'' while that of Samp2 is 130''. Annealing improves the crystallinity but the broader shoulders of the annealed sample shows other defects may evolve during the annealing. Figure 6(c) shows the comparison of calculated and measured thermal conductivity. The four samples studied in this work were heated to 450 °C during the exfoliation process. Samp2 and Samp4 were annealed at 800 °C in N₂. The 450 °C heating drives the H ions out of β -Ga₂O₃ films while the high temperature annealing (800 °C) can improve the quality of the films by reducing the amounts of defects (vacancies) in the films. Phonons scatter with defects due to mass difference, and the local strain which induces changes in local bond stiffness, lattice constant, and Gruneisen parameter.²⁷ If we do not consider mass difference, then the local strain field is the primary source for phonon-defect scatterings, similar to other implanted materials.²⁷ The strain-induced phonon-defect scatterings reduce the thermal conductivity of these β -Ga₂O₃ thin films. The line labeled with "No strain" in Figure 6(c) shows the thickness dependent thermal conductivity which only considers the phonon-phonon scatterings and phonon-boundary scatterings. The measured thermal conductivity is slightly lower than the calculated thermal conductivity because of the remaining small amount of structural imperfection, which was confirmed by the shoulder in the XRD curve. The line labeled with "Strain" in Figure 6(c) shows the thickness dependent thermal conductivity which adds additional phonon-defect scatterings. By adding the phonon-defect scatterings into the calculation, we can match the measured thermal conductivity of the as-bonded samples to obtain the scattering cross-section (Γ_i) as 0.3. The phonon scattering mechanisms are shown in Figure 6(d). The strain field induced phonon-defect scattering exists in the films while the phonon-boundary scatterings happen at the film boundaries. Both the phonon-boundary scatterings and phonon-defect scatterings reduce thermal conductivity of these

thin films. The phonon-phonon scatterings are not included in the figure because they exist in both the films with strain and films without strains.

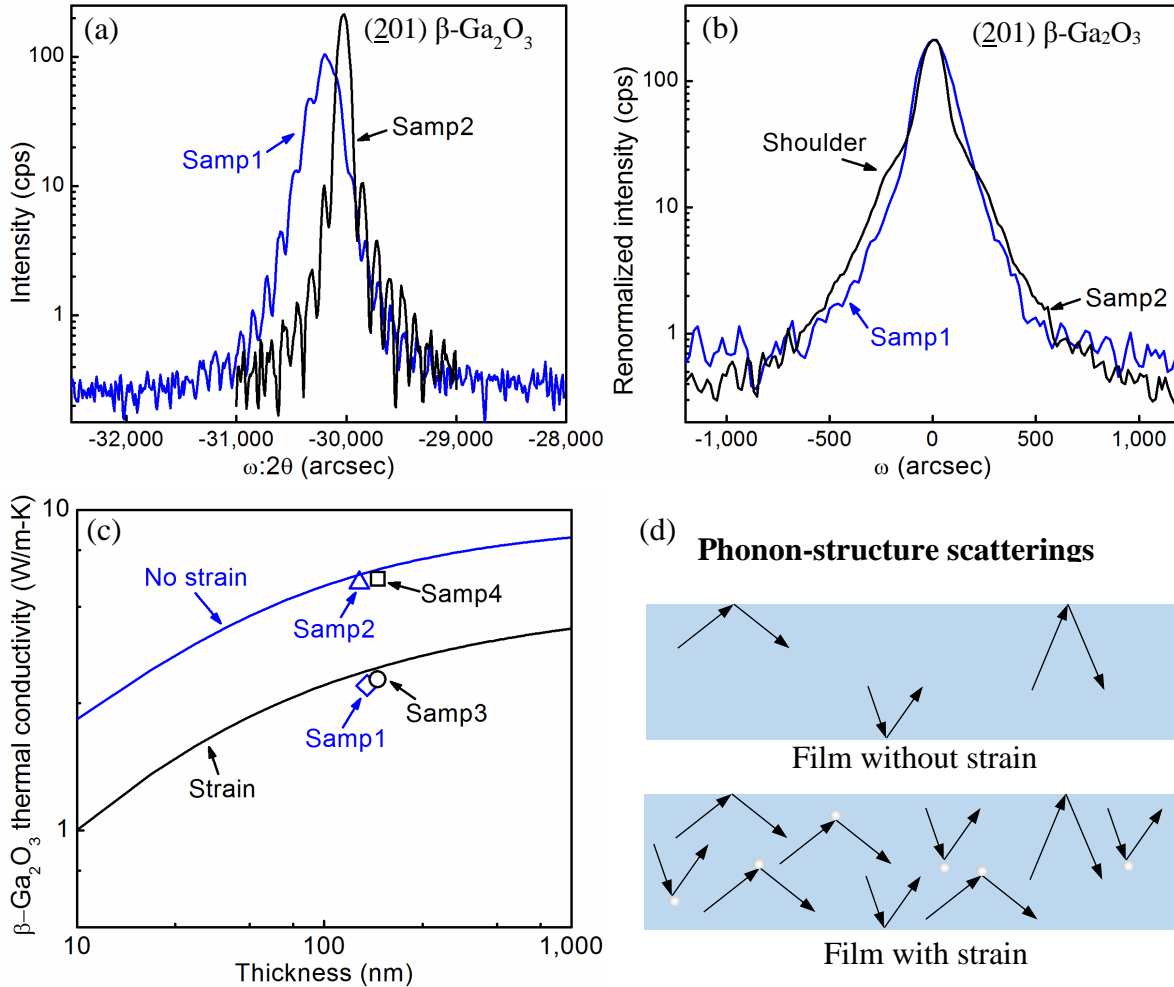


Figure 6. (a) Triple-axis ($\omega:2\theta$) scans of Samp1 and Samp2. (b) Triple-axis rocking curves of Samp1 and Samp2. The FWHM of Samp1 is $170''$ while that of Samp2 is $130''$. (c) Comparison of calculated and measured thermal conductivity of $\beta\text{-Ga}_2\text{O}_3$ thin films. (d) Phonon scatterings with film boundaries and defects. The strain in the as-bonded samples induces phonon-defect scattering and correspondingly reduce thermal conductivity.

Conclusions

This work reports a scalable thermal management strategy to heterogeneously integrate wafer-scale monocrystalline β -Ga₂O₃ thin films on high thermal conductivity 4H-SiC substrates by ion-cutting and surface activated bonding techniques. We observe medium TBC values (67-100 MW/m²-K) of the β -Ga₂O₃-SiC interfaces. The TBC values increase about 39% and 32% when decreasing the Al₂O₃ interlayer thickness from 30 nm to 10 nm for the as-bonded and annealed interfaces, respectively. The thermal annealing reduces the β -Ga₂O₃-SiC TBC slightly possibly due to Ga element or GaO_x diffusion into the Al₂O₃ interlayer. The β -Ga₂O₃ thermal conductivity increases by a factor of two after annealing in N₂ at 800 °C due to the removal of implantation-induced strain in the films. Some theoretical models were used to understand the measured TBC and thermal conductivity. Fourteen different spots were measured to evaluate the uniformity. The small spot-spot variations of both TBC and β -Ga₂O₃ thermal conductivity confirm the uniformity and effectiveness of the bonding, exfoliation, and annealing. Our work paves the way for thermal management of power electronics and β -Ga₂O₃ related semiconductor devices.

Methods

Sample Preparation. The on-axis (0001) 4-inch 4H-SiC wafers with a thickness of ~500 μ m were purchased from SICC Co., Ltd. The (201) 2-inch β -Ga₂O₃ wafers with a thickness ~680 μ m were purchased from Novel Crystal Technology Inc. The Si-face of the 4H-SiC was used as the bonding surface. All of the bonding surfaces were polished by chemical mechanical polishing (CMP). The root-mean-square (RMS) surface roughness of the SiC and β -Ga₂O₃ surfaces are ~0.30 nm and ~0.27 nm, respectively.

The thin film exfoliation can be achieved by either hydrogen or helium ion implantation.²⁸ In the present study, the β -Ga₂O₃ wafers were implanted by hydrogen ions (H⁺) with a 7-degree tilt to minimize the ion channeling effect.²⁹ The implanted H⁺ ions accumulate in the β -Ga₂O₃ at 200-400 nm beneath the surface. After the ion implantation, an Al₂O₃ film was deposited on the Ga₂O₃ wafers by plasma-enhanced atom-layer deposition (PEALD) to avoid the surface damage layer during the following surface activation process for bonding and also blocking possible electrical breakdown due to the defective interfaces. Trimethylaluminum (TMA) and O₂ plasma were used as ALD precursors. Ar gas flow served as both carriers and purging gas. The O₂ plasma power was 100 W. The total flow rate of the Ar was 200 sccm (standard cubic centimeters per minute). The Al₂O₃ thin films were grown at 200 °C. The growth rate per cycle (GPC) was typically 1.3 Å/cycle for Al₂O₃. Al₂O₃ films with two kinds of thickness (30 nm for Samp1 and Samp2 and 10 nm for Samp3 and Samp4) were deposited on the implanted β -Ga₂O₃ wafers. After that, the two wafers were bonded together at room temperature by the surface-activated bonding (SAB) technique. The SAB machine consists of a load-lock chamber and a processing-bonding chamber. A silicon source is placed in the ion source to generate a mixture of Si ions and Ar ions. The small amount of Si ions added into the Ar ion beam was aimed to reduce the carbonation of SiC surface during the ion beam bombardment. The Ar ions activate the SiC and Al₂O₃ (on the β -Ga₂O₃) surfaces to create dangling bonds. After the surface activation, the samples were bonded directly at room temperature. The detailed bonding process can be found in the literature.³⁰

By heating the bonded wafers at 450 °C, the implanted H⁺ ions accumulate near the projected range of the ion implantation to induce the exfoliation of a β -Ga₂O₃ thin film.^{26,29,31,32} After that, a β -Ga₂O₃ thin film with a thickness of less than 400 nm was split from the bulk β -Ga₂O₃ wafer and

transferred to SiC substrate. The exfoliated β -Ga₂O₃ thin film was thinned by CMP to obtain a good TDTR sensitivity of the buried β -Ga₂O₃-SiC interface (100-200 nm thick). The post-exfoliated β -Ga₂O₃ bulk wafer can be repeatedly used for multiple exfoliations after polishing. The transferred 2-inch β -Ga₂O₃-on-SiC wafers were diced into 10 mm × 8 mm chips. Some chips were annealed in flowing N₂ gas. The temperature was ramped to 800 °C with a rate of 5 °C/min and then held at 800 °C for 30 min. Finally, a ~100-nm-thick Al TDTR transducer layer was deposited on the surface of all samples.

TDTR Measurements. TDTR is a femtosecond-laser-based optical pump-probe technique to measure thermal properties of both bulk and nanostructured materials.^{9,20} A modulated pump beam heats the sample surface periodically while a delayed probe beam detects the surface temperature variation via thermoreflectance.²² The variation of surface temperature is fitted with an analytical heat transfer solution of the samples to infer the unknown thermal parameters.^{10,22} The measurements in this work are similar to those in references.^{10,11,33,34}

A 10 X objective (pump radius 10.1 μm and probe radius 5.8 μm) is used for the measurements with modulation frequency of 2.2 MHz. The low modulation frequency is to obtain deep thermal penetration depth to get enough sensitivity for the buried β -Ga₂O₃- SiC interfaces. More information about TDTR sensitivity can be found in the Supplementary Information. A bare SiC wafer was measured first to obtain the SiC thermal conductivity (337 W/m-K), which was used as a known parameter in the data fitting of measurements on β -Ga₂O₃ on SiC samples. The Al and β -Ga₂O₃ thicknesses were measured by the picosecond acoustic technique and confirmed with TEM results. The thermal conductivity of Al is obtained by measuring the electrical conductivity and

applying Wiedemann-Franz law. The heat capacity of the Al transducer, the β -Ga₂O₃ thin film, and the SiC substrates are from literature.^{22,24,33,35}

Materials Characterization. Cross-section TEM samples were prepared with a FEI Helios dual beam focused ion beam (FIB) system. The interfacial structures were characterized by a HR-STEM (Probe-corrected FEI Titan) and the interfacial composition was measured by EELS (Gatan Enfinium). The observation in this study is along $\langle 11-20 \rangle$ axis of SiC and $\langle 010 \rangle$ axis of β -Ga₂O₃. Triple-axis x-ray diffraction measurements were performed on a Bruker-JV D1 high-resolution X-ray diffractometer with incident beam conditioning that includes a parallel beam optical element and a (110) channel-cut silicon crystal that produces a monochromatic, highly collimated Cu K α_1 beam. The scattered beam optics also included a (110) channel-cut silicon crystal. Both longitudinal ($\Delta(\omega:2\theta)$) scans and rocking curves ($\Delta\omega$) were recorded under these triple axis HRXRD conditions.

Theoretical Modelings. A Landauer approach with DMM is used to calculate the β -Ga₂O₃-Al₂O₃, Al₂O₃-SiC, and β -Ga₂O₃-SiC TBC. Because the transmission function from DMM does not depend on the angle of incidence, the Landauer formula is:

$$G = \sum_v \frac{1}{4} \int D_1(\omega) \frac{df_{BE}}{dT} \hbar \omega v_1(\omega) \tau_{12}(\omega) d\omega. \quad (1)$$

where D is the phonon density of states, f_{BE} is the Bose-Einstein distribution function, \hbar is the reduced Planck constant, ω is the phonon angular frequency, v is the phonon group velocity of material 1, τ_{12} is the transmission coefficient from material 1 to 2, and the sum is over all incident phonon modes. The expression of the transmission function from DMM²³ is

$$\tau_{12}(\omega) = \frac{\sum_p M_2(\omega)}{\sum_p M_1(\omega) + \sum_p M_2(\omega)}, \quad (2)$$

where M is the phonon number of modes. The phonon properties of diamond are obtained from first principles calculation with VASP.

A Callaway model is used to understand the measured β -Ga₂O₃ thermal conductivity by taking account of the film boundary scattering and strain effect in the films.³⁶⁻³⁸ The phonon dispersion relation of β -Ga₂O₃ is calculated by density-functional-theory (DFT). All the phonon polarizations are considered (acoustic and optical, totally 30 branches for β -Ga₂O₃). The Callaway model gives an expression of thermal conductivity k as an integration in frequency space:

$$k = \frac{1}{3} \sum_p \int_0^{\omega_{\text{cut-off}}} \hbar \omega D_\lambda \frac{df_{BE}}{dT} v_\lambda^2 \tau_{C,\lambda}, \quad (3)$$

where the 1/3 comes from the isotropic assumption, \sum_p is over all phonon polarizations, v_λ is the modal phonon group velocity, $\tau_{C,\lambda}$ is the modal combined relaxation time of phonon mode λ , D_λ is the modal phonon density of states, and f_{BE} is the Bose-Einstein distribution function. Three phonon scattering mechanisms are included in our calculation: phonon-phonon scatterings, phonon-boundary scatterings, and phonon-defect scatterings. The effective relaxation time $\tau_{C,\lambda}$ of each phonon mode can be obtained from the Matthiessen's rule³⁸:

$$\tau_{C,\lambda} = \left(\frac{1}{\tau_U} + \frac{1}{\tau_D} + \frac{1}{\tau_B} \right)^{-1} \quad (4)$$

where τ_U , τ_D , and τ_B are the relaxation time of Umklapp phonon-phonon scatterings, phonon-defect scatterings, and phonon-boundary scatterings, respectively. The scattering rate can be shown below.^{27,39}

$$\frac{1}{\tau_U} = BT\omega^2 e^{-\frac{c}{T}}, \quad (5)$$

$$\frac{1}{\tau_D} = \frac{V\omega^4}{4\pi v^3} \Gamma_i, \quad (6)$$

$$\frac{1}{\tau_B} = v/d, \quad (7)$$

where B and C are fitting parameters, V is the atomic volume of the β -Ga₂O₃, Γ_i is the parameter to describe the strength of phonon-defect scattering of defect i , and d is the thickness of the β -Ga₂O₃ film. When calculating the scattering rates of different mechanisms, the B (2.3×10^{-18} s/K) and C (130 K) are obtained by fitting with the previous experimental measurements.^{8,24}

Competing interests: The authors claim no competing financial interests.

Author contributions: Z. C., J. S., and S. G. did the thermal measurements and calculations. F. M., T. Y., W. X., T. S., and X. O. fabricated the samples and finished part of the material characterizations. M. E. L., Y. W., K. H., and M. S. G. finished the XRD measurements and part of the TEM study. Z. C. wrote the manuscript with inputs from all other authors.

Acknowledgements: Z. C., J. S., M. E. L., Y. W., K. H., M. S. G., and S. G. would like to acknowledge the financial support from U.S. Office of Naval Research under a MURI program (Grant No. N00014-18-1-2429). Z. C. J. S., and S. G. acknowledge the funding support from U.S. Air Force Office of Scientific Research under a MURI program (Grant No. FA9550-18-1-0479). F.M., and T.S. would like to acknowledge the financial support from Japan JSPS KAKENHI Grant Number 19K15298 and the Precise Measurement Technology Promotion Foundation. T. Y., W. X., and X. O. was supported by National Natural Science Foundation of China (No. 61874128, 61851406, and 11705262), Frontier Science Key Program of CAS (No. QYZDY-SSW-JSC032), and Shanghai Science and Technology Innovation Action Plan Program (No. 17511106202).

References

- 1 Liu, Y. *et al.* van der Waals Integrated Devices Based on Nanomembranes of 3D Materials. *Nano Letters* **20**, 1410-1416 (2020).
- 2 Higashiwaki, M. & Jessen, G. H. (AIP Publishing, 2018).
- 3 Pearton, S. *et al.* A review of Ga₂O₃ materials, processing, and devices. *Applied Physics Reviews* **5**, 011301 (2018).
- 4 Reese, S. B., Remo, T., Green, J. & Zakutayev, A. How Much Will Gallium Oxide Power Electronics Cost? *Joule* (2019).
- 5 Higashiwaki, M., Sasaki, K., Kuramata, A., Masui, T. & Yamakoshi, S. Gallium oxide (Ga₂O₃) metal-semiconductor field-effect transistors on single-crystal β -Ga₂O₃ (010) substrates. *Applied Physics Letters* **100**, 013504 (2012).
- 6 Tsao, J. *et al.* Ultrawide-Bandgap Semiconductors: Research Opportunities and Challenges. *Advanced Electronic Materials* **4**, 1600501 (2018).
- 7 Cheng, Z. *et al.* Significantly Reduced Thermal Conductivity in Beta-(Al_{0.1}Ga_{0.9})₂O₃/Ga₂O₃ Superlattices. *Applied Physics Letter* **115** (2019).
- 8 Jiang, P., Qian, X., Li, X. & Yang, R. Three-dimensional anisotropic thermal conductivity tensor of single crystalline β -Ga₂O₃. *Applied Physics Letters* **113**, 232105 (2018).
- 9 Cheng, Z. *et al.* Experimental observation of high intrinsic thermal conductivity of AlN. *Physical Review Materials* **4**, 044602 (2020).
- 10 Cheng, Z., Mu, F., Yates, L., Suga, T. & Graham, S. Interfacial Thermal Conductance across Room-Temperature-Bonded GaN/Diamond Interfaces for GaN-on-Diamond Devices. *ACS Applied Materials & Interfaces* **12**, 8376-8384 (2020).

- 11 Cheng, Z. *et al.* Thermal conductance across β -Ga₂O₃-diamond van der Waals heterogeneous interfaces. *APL Materials* **7**, 031118 (2019).
- 12 Cheng, Z. *et al.* Integration of polycrystalline Ga₂O₃ on diamond for thermal management. *Applied Physics Letters* **116**, 062105 (2020).
- 13 Mu, F. *et al.* High Thermal Boundary Conductance across Bonded Heterogeneous GaN–SiC Interfaces. *ACS applied materials & interfaces* **11**, 33428-33434 (2019).
- 14 Aller, H. T. *et al.* Chemical Reactions Impede Thermal Transport Across Metal/ β -Ga₂O₃ Interfaces. *Nano letters* **19**, 8533-8538 (2019).
- 15 Hwang, W. S. *et al.* High-voltage field effect transistors with wide-bandgap β -Ga₂O₃ nanomembranes. *Applied Physics Letters* **104**, 203111 (2014).
- 16 Ahn, S. *et al.* Effect of front and back gates on β -Ga₂O₃ nano-belt field-effect transistors. *Applied Physics Letters* **109**, 062102 (2016).
- 17 Zhou, H., Maize, K., Qiu, G., Shakouri, A. & Ye, P. D. β -Ga₂O₃ on insulator field-effect transistors with drain currents exceeding 1.5 A/mm and their self-heating effect. *Applied Physics Letters* **111**, 092102 (2017).
- 18 Kim, J., Mastro, M. A., Tadjer, M. J. & Kim, J. Heterostructure WSe₂– Ga₂O₃ Junction Field-Effect Transistor for Low-Dimensional High-Power Electronics. *ACS applied materials & interfaces* **10**, 29724-29729 (2018).
- 19 Noh, J., Si, M., Zhou, H., Tadjer, M. J. & Peide, D. Y. in *2018 76th Device Research Conference (DRC)*. 1-2 (IEEE).
- 20 Cahill, D. G. Analysis of heat flow in layered structures for time-domain thermoreflectance. *Review of scientific instruments* **75**, 5119-5122 (2004).

- 21 Cheng, Z. *et al.* Probing Growth-Induced Anisotropic Thermal Transport in High-Quality CVD Diamond Membranes by Multi-frequency and Multi-spot-size Time-Domain Thermoreflectance. *ACS applied materials & interfaces* (2018).
- 22 Cheng, Z. *et al.* Tunable Thermal Energy Transport across Diamond Membranes and Diamond-Si Interfaces by Nanoscale Graphoepitaxy. *ACS applied materials & interfaces* (2019).
- 23 Fisher, T. S. *Thermal energy at the nanoscale*. Vol. 3 (World Scientific Publishing Company, 2013).
- 24 Guo, Z. *et al.* Anisotropic thermal conductivity in single crystal β -gallium oxide. *Applied Physics Letters* **106**, 111909 (2015).
- 25 Scott, E. A. *et al.* Orders of magnitude reduction in the thermal conductivity of polycrystalline diamond through carbon, nitrogen, and oxygen ion implantation. *Carbon* **157**, 97-105 (2020).
- 26 Miclaus, C. & Goorsky, M. Strain evolution in hydrogen-implanted silicon. *Journal of Physics D: Applied Physics* **36**, A177 (2003).
- 27 Scott, E. A. *et al.* Phonon scattering effects from point and extended defects on thermal conductivity studied via ion irradiation of crystals with self-impurities. *Physical Review Materials* **2**, 095001 (2018).
- 28 Liao, M. E., Wang, Y., Bai, T. & Goorsky, M. S. Exfoliation of β -Ga₂O₃ Along a Non-Cleavage Plane Using Helium Ion Implantation. *ECS Journal of Solid State Science and Technology* **8**, P673-P676 (2019).
- 29 Xu, W. *et al.* in *2019 IEEE International Electron Devices Meeting (IEDM)*. 12.15. 11-12.15. 14 (IEEE).

- 30 Xu, Y. *et al.* Direct wafer bonding of Ga₂O₃–SiC at room temperature. *Ceramics International* **45**, 6552-6555 (2019).
- 31 Hayashi, S., Bruno, D. & Goorsky, M. Temperature dependence of hydrogen-induced exfoliation of InP. *Applied Physics Letters* **85**, 236-238 (2004).
- 32 Ferain, I., Byun, K. Y., Colinge, C., Brightup, S. & Goorsky, M. Low temperature exfoliation process in hydrogen-implanted germanium layers. *Journal of Applied Physics* **107**, 054315 (2010).
- 33 Mu, F. *et al.* High Thermal Boundary Conductance across Bonded Heterogeneous GaN–SiC Interfaces. *ACS Applied Materials & Interfaces* **11**, 7 (2019).
- 34 Gaskins, J. T. *et al.* Thermal Boundary Conductance Across Heteroepitaxial ZnO/GaN Interfaces: Assessment of the Phonon Gas Model. *Nano letters* **18**, 7469-7477 (2018).
- 35 Zheng, Q. *et al.* Thermal conductivity of GaN, GaN 71, and SiC from 150 K to 850 K. *Physical Review Materials* **3**, 014601 (2019).
- 36 Callaway, J. Model for lattice thermal conductivity at low temperatures. *Physical Review* **113**, 1046 (1959).
- 37 Mingo, N. Calculation of Si nanowire thermal conductivity using complete phonon dispersion relations. *Physical Review B* **68**, 113308 (2003).
- 38 Feng, T. & Ruan, X. Quantum mechanical prediction of four-phonon scattering rates and reduced thermal conductivity of solids. *Physical Review B* **93**, 045202 (2016).
- 39 Klemens, P. The scattering of low-frequency lattice waves by static imperfections. *Proceedings of the Physical Society. Section A* **68**, 1113 (1955).